

Photochemical Activation of a Hydroxyquinone-Derived Phenyliodonium Ylide by Visible Light: Synthetic and Mechanistic Investigations

Mona Jalali, Curtis C. Ho, Rebecca O. Fuller, Nigel T. Lucas, Alireza Ariaifard,* and Alex C. Bissember*

Cite This: *J. Org. Chem.* 2021, 86, 1758–1768

Read Online

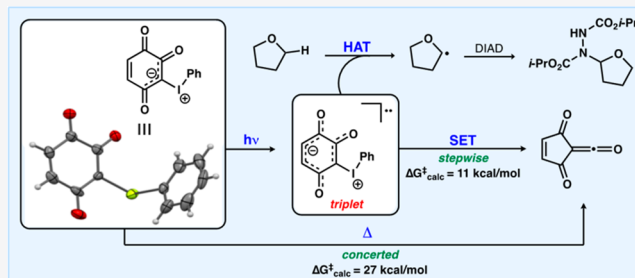
ACCESS |

Metrics & More

Article Recommendations

Supporting Information

ABSTRACT: We have identified and extensively investigated the photochemical activation and reaction of a hydroxyquinone-derived phenyliodonium ylide in the presence of visible light using experiment and theory. These studies revealed that in its photoexcited state this iodonium is capable of facilitating a range of single-electron transfer (SET) processes, including hydrogen atom transfer (HAT), a Povarov-type reaction, and atom-transfer radical addition chemistry. Where possible, we have employed density functional theory (DFT) to develop a more complete understanding of these photoinduced synthetic transformations.



INTRODUCTION

Zwitterionic hydroxyquinone-derived phenyliodonium ylides, such as molecules **1**, are an established class of compounds that are air-stable, both in solution and the solid state (Figure 1).^{1–3} The X-ray crystallographic characterization of lawsone derivative **1b** confirms that this structure is zwitterionic consisting of a positively charged iodine atom and a negative charge delocalized across three contiguous carbon centers.³ These hydroxyquinone-derived iodoniums can engage in synthetically useful bimolecular reactions, such as transition-metal-catalyzed cross-couplings with organometallic nucleophiles, other C–C bond-forming reactions, and formal cycloadditions.⁴ However, ylides such as compound **1a** are particularly susceptible to thermally promoted intramolecular rearrangements.² These processes furnish cyclopentenones via putative cyclic ketenes (Figure 1A). Although highly reactive ketenes, such as species **2a**, have not been isolated, their existence is supported by both experiment and theory.^{2b,5,6}

We recognized that hydroxyquinone-derived phenyliodonium ylides **1** represent a relatively underutilized class of compounds in synthesis. In response, we sought to explore and extend the synthetic applications of these types of molecules accordingly. Specifically, we wanted to investigate the capacity for visible light to activate these systems and further unlock their potential. It was recently reported that β -dicarbonyl-derived iodonium ylides, such as **1d**, engage in cyclopropanation reactions with olefins in the presence of visible light (Figure 1B),⁷ which contrasts with the formation of dihydrofuran products when UV irradiation is employed.⁸ In this work, we employ experiment and theory to study the fundamental reactivity of related molecule **1a** in the ground-

and excited-states and explore the viability of phenyliodonium **1a** to promote single electron-transfer processes induced by visible light.

RESULTS AND DISCUSSION

First, we prepared hydroxyquinone-derived phenyliodonium ylide **1a** on an 11-g scale (72% yield) from commercially available 1,2,4-trihydroxybenzene in one step (Figure 2A).^{2b} We also confirmed the structure of compound **1a** by single crystal X-ray crystallography for the first time (Figure 2B). This established that the structure of molecule **1a** is consistent with that of lawsone-derived phenyliodonium **1b**.³ We observed that the asymmetric unit contains two crystallographically independent molecules that differ insignificantly in their geometric parameters. The molecules display biaxial noncovalent interactions between the iodine atom of one molecule and the carbonyl oxygen atoms of another (I1...O4, O5 2.828, 3.132 Å).

The traditional approach of using close contacts to elucidate packing and structural features can be greatly enhanced through the visualization of the electrostatic potential distribution for the determined crystallographic structure.⁹ We mapped the electrostatic potential at HF 3-21G onto an electron density isosurface in which areas of blue are associated

Received: October 30, 2020

Published: December 30, 2020



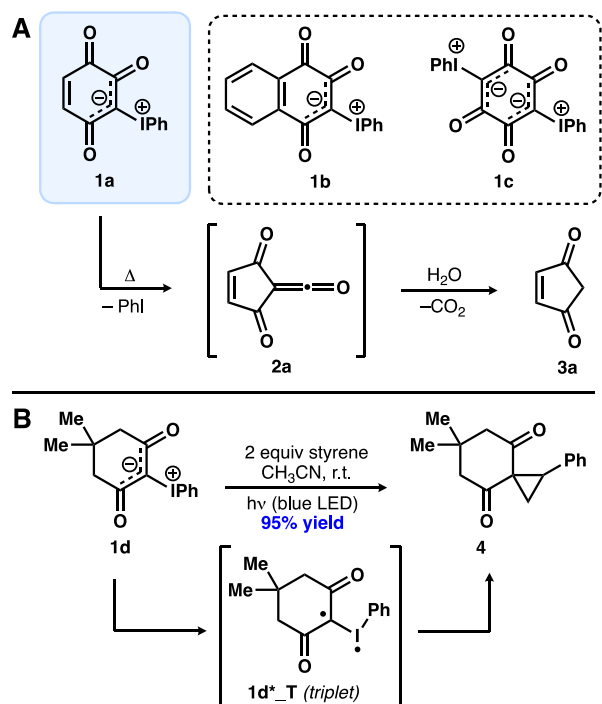


Figure 1. (A) Representative hydroxyquinone-derived phenyliodonium ylides and thermally promoted formation of cyclopentenedione **3a** from phenyliodonium **1a**. (B) Reported photoinduced cyclopropanation of phenyliodonium **1d**.⁷

with positive regions of the surface with red assigned as negative electrostatic potential (Figure 2C). This highlights that these close contacts are likely to involve the electropositive region of the iodine and neighboring negative potential of the oxygen atoms. The biaxial coordination of the neighboring iodonium compound appears to primarily arise from the electrostatic complementarity of the neighboring molecules.¹⁰ The most positive part of the surface is associated with the phenyl group of the adjacent molecule. Notably, we could not find evidence of a binding mode consistent with a halogen bond donor/acceptor pair. Such interactions have recently been invoked for germane supramolecular structures comprising hypervalent iodine(III) molecules and chelating Lewis bases.¹¹

Thermal Activation of Ylide 1a. Next, we resolved to use theory and experiment to better understand the thermally promoted transformation of iodonium **1a** to ketene **2a**. By monitoring the consumption of substrate **1a** via ¹H NMR spectroscopy, we observed that phenyliodonium **1a** does not undergo reaction in acetonitrile at ambient temperature in the dark over 24 h (Table 1, entry 1).¹² This reaction proceeds relatively slowly at 40 °C (entries 2 and 3) and much faster at 60 and 80 °C as one might expect (entries 4 and 5). The consumption of molecule **1a** is faster in chloroform (entries 6–8), a nonpolar solvent, and was not inhibited by the presence of TEMPO (entry 9). These observations are consistent with the absence of SET processes under these conditions. We attempted to trap ketene **2a** as its corresponding (dppf)nickel-(ketene) adduct;¹³ however, despite considerable experimentation, all efforts to isolate such a complex were not successful.

In 2008, a DFT study employing B3LYP level of theory in the gas phase proposed that this transformation proceeds via a concerted mechanism involving a 4-membered [1.1.0] cyclic

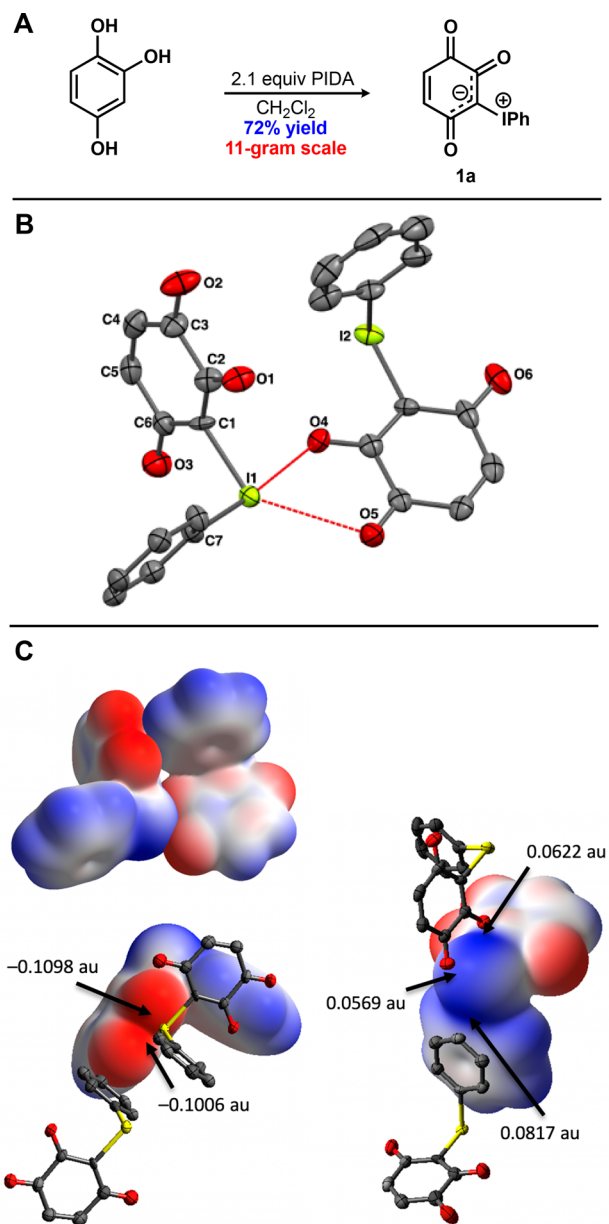
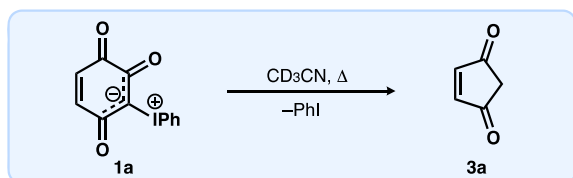


Figure 2. (A) Synthesis of phenyliodonium ylide **1a**; PIDA = (diacetoxyiodo)benzene. (B) Structural representation of molecule **1a** with thermal ellipsoids drawn at the 50% probability level and hydrogen atoms are omitted for clarity: Selected bond lengths (Å) and angles (deg): I1–C1,C7 2.076(5), 2.117(5), C1–C2,C6 1.383(7), 1.432(8), C2–O1,C3 1.261(6), 1.549(7), C3–O2,C4 1.223(7), 1.461(8), C4–C5 1.327(8), C6–O3,C5 1.230(7), 1.491(8), C1–I1–C7 94.9(2). (C) Electrostatic complementarity for neighboring phenyliodonium molecules **1a** interpreted via the mapping of the electrostatic potentials on 0.002 au isosurfaces of the electron density calculated with HF 3-21G wave functions. Values between -0.05 au (red) and $+0.05$ au (blue) have been mapped; 1 au = 2627.21 kJ/mol.

transition state (**1a** \rightarrow **2a**: $\Delta G_{\text{calc}}^\ddagger = 11.6$ kcal/mol).^{6,14} These calculations, which suggest an extremely low activation energy barrier for this process, appear inconsistent with many of the results shown in Table 1 and previous experiments reporting the thermal reaction of phenyliodonium **1a**.^{2b} We noted that in a recent study exploring the mechanism of an IBX-mediated oxidation reaction it was determined that the M06-2X functional predicts energies of hypervalent iodine species

Table 1. Thermal Reaction of Phenyliodonium 1a: Influence of Reaction Parameters^a



entry	variation	time (h)	yield (%) ^b
1	24 °C	24	0 (0)
2	40 °C	1	21 (37)
3	40 °C	2	41 (45)
4	60 °C	1	97 (100)
5	80 °C	0.25	90 (100)
6	in CDCl ₃ , 40 °C	0.5	17 (20)
7	in CDCl ₃ , 40 °C	1	39 (44)
8	in CDCl ₃ , 40 °C	2	80 (87)
9 ^c	40 °C	2	40 (45)

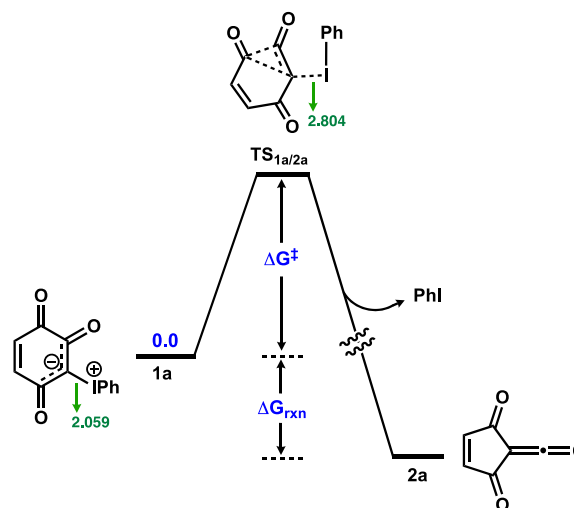
^aReactions were performed in the dark employing 12.3 μmol **1a**, [0.03 M]. ^bYield of **3a** determined by ¹H NMR spectroscopy with the aid of a calibrated internal standard (average of 2 experiments). ^cPerformed in the presence of TEMPO (2 equiv); consumption of **1a** is shown in parentheses.

more accurately than other DFT methods, including B3LYP.¹⁵ Consequently, we investigated the transformation of **1a** → **2a** using the M06-2X functional while also accounting for the role of solvent in this reaction.¹⁶ The respective free energies of activation for the thermal process starting from iodonium **1a** determined via this approach were higher than equivalent results obtained at the B3LYP level (Table 2). Specifically, these data suggest that the activation energy barriers are underestimated by the B3LYP level of theory. We determined that $\Delta G^\ddagger = 27.5$ kcal/mol for **1a** → **2a** in CD₃CN using SMD/CCSD(T)/BS2//SMD/M06-2X-D3/BS1 calculations and this further supports the higher accuracy of the M06-2X method in predicting the barrier height. Our calculations also reveal that formation of ketene **2a** from **1a** is exergonic (ca. -40 kcal/mol), which is consistent with the irreversible nature of the process.

Although formation of molecule **2a** from iodonium **1a** is thermodynamically favorable, our DFT calculations are consistent with ketene **2a** being particularly sensitive to moisture (Figure 3).¹⁷ Specifically, the addition of a water molecule to ketene **2a** requires minimal free energy of activation ($\Delta G^\ddagger = 8.5$ kcal/mol) and affords enol **B** in an exergonic fashion ($\Delta G = -9.0$ kcal/mol). Intermediate **B** is predicted to be in equilibrium with zwitterion **D**. The reaction of the latter with a water molecule then produces species **F**. This is followed by the rate-determining decarboxylation step that likely affords species **G** ($\Delta G^\ddagger = 24.4$ kcal/mol). Surmounting this relatively high activation energy barrier is consistent with the need to heat the reaction above ambient temperature to facilitate an efficient reaction (Table 1). Finally, we propose that product **3a** is obtained from intermediate **G** following another proton transfer step involving water.

Photochemical Activation of Ylide 1a. We determined that the absorption maximum for molecule **1a** is 439 nm employing UV-vis spectroscopy.¹⁸ This prompted us to investigate the capacity for visible light to facilitate the photochemical activation of this phenyliodonium. We monitored the reaction of substrate **1a** in the presence of

Table 2. Free Energies of Activation (ΔG^\ddagger) and Reaction (ΔG_{rxn}) Calculated at Different Levels of Theory and Solvents for Transformation of **1a → **2a**^a**



optimization method	single point method	solvent	ΔG^\ddagger	ΔG_{rxn}
SMD/B3LYP-D3/BS1	SMD/B3LYP-D3/BS2	CD ₃ CN	18.4	-41.8
		CDCl ₃	20.6	-42.1
SMD/M062X-D3/BS1	SMD/M062X-D3/BS2	CD ₃ CN	27.0	-41.3
		CDCl ₃	26.3	-42.3

^aSelected bond distances (green) and free energies are given in Å and kcal/mol (referenced to compound **1a**), respectively. BS1 = LANL2DZ,6-31G(d) and BS2 = def2-TZVP.

visible light at 0 °C via ¹H NMR spectroscopy and observed the rapid consumption of this compound within 45 min (Table 3, entries 1–3). No reaction occurred in the absence of light, the consumption of molecule **1a** was much slower in a polar solvent, and the consumption of **1a** still occurred at -50 °C (entries 4–8). Notably, in all of these experiments, product **3a** was not formed. However, dione **3a** could be synthesized when substrate **1a** was irradiated in acetonitrile at 40 °C (entry 10). Control experiments suggest that the formation of product **3a** occurs by both thermal and photochemical pathways under these conditions (Table 1, entry 2 vs Table 3, entry 10). Interestingly, while the consumption of substrate **1a** decreased in the presence of TEMPO and visible light, a similar yield of dione **3a** was obtained under these conditions (Table 3, entry 11).

We employed TD-DFT calculations at the CAM-B3LYP level of theory to investigate the mechanism of photoactivation for iodonium **1a** and understand why irradiation with visible light appears to accelerate the transformation **1a** → **3a** (Figure 4A). Although our studies revealed the existence of a band at 440 nm, the oscillator strength was negligible. However, the second excitation at 380 nm was identified, which corresponds to the transition of an electron from the HOMO to the LUMO of substrate **1a** (Figure 4B). Specifically, this involves the transfer of an electron from the nonbonding lone pair on C¹ atom to the C³=C⁴ π* orbital (oscillator strength of $f = 0.03$).¹⁹ Due to the nature of this charge transfer, the optimization of this excited state gives a structure in which the I–C bonds are largely intact (see the structural parameters for species **1a** and **1a***; Figure 4A). The ensuing excited structure was then used as an initial starting point for geometry

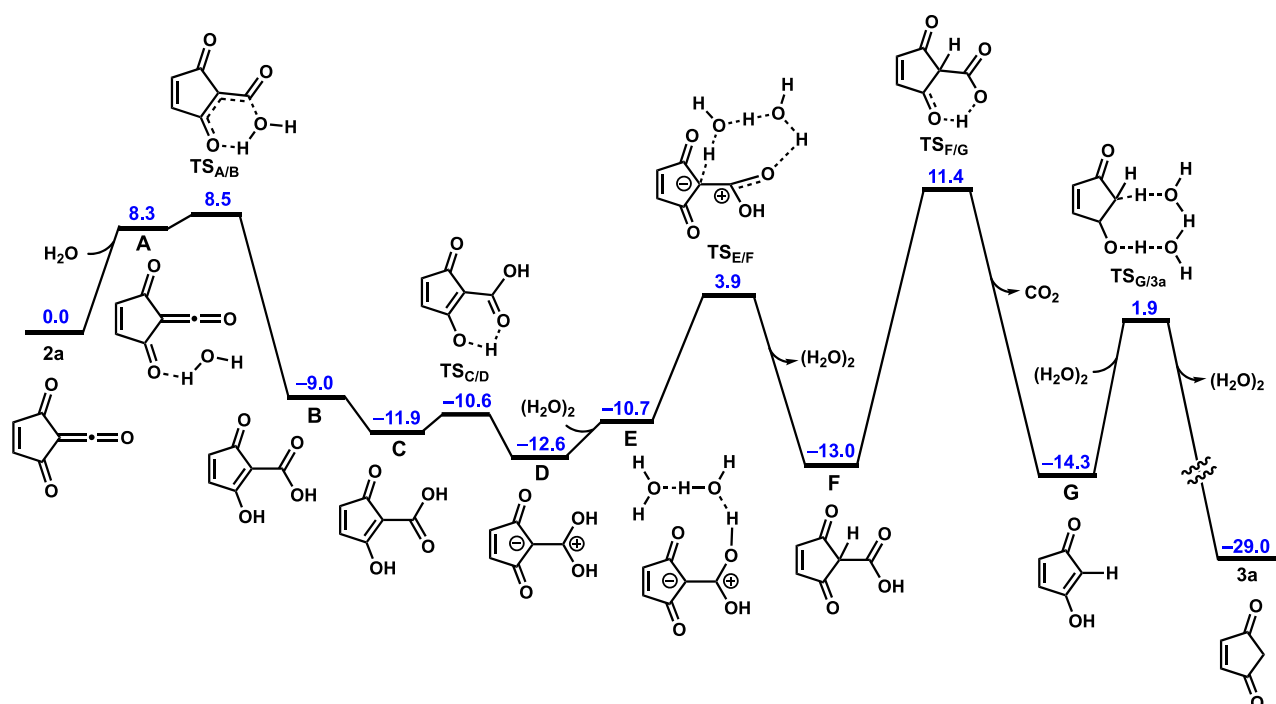
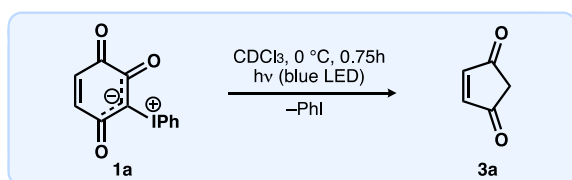


Figure 3. A free energy profile for the conversion of **2a** → **3a** calculated by BS1 = LANL2DZ,6-31G(d) and BS2 = def2-TZVP. Free energies are given in kcal/mol and referenced to compound **2a**.

Table 3. Reaction of Phenyliodonium **1a** in the Presence of Visible Light: Influence of Reaction Parameters^a



entry	variation	time (min)	yield (%) ^b
1	none	45	<1 (100)
2	none	30	<1 (90)
3	none	15	<1 (50)
4	no <i>hν</i>	45	0 (0)
5	in CD ₃ CN	15	<1 (9)
6	in CD ₃ CN	30	<1 (22)
7	in CD ₃ CN	60	<1 (38)
8	-50 °C	150	<1 (41)
9	40 °C	60	<1 (100)
10	in CD ₃ CN, 40 °C	60	50 (100)
11 ^c	in CD ₃ CN, 40 °C	60	56 (73)

^aReactions performed employing 12.3 μmol **1a**, [0.03 M]; blue LED $\lambda_{\text{max}} = 467$ nm. ^bYield of **3a** determined by ¹H NMR spectroscopy with the aid of a calibrated internal standard (average of 2 experiments). ^cPerformed in the presence of TEMPO (2 equiv); consumption of **1a** is shown in parentheses.

optimization of the triplet state and negligible change in the I–C bond distances was observed upon moving from intermediate **1a*** to **1a*_T**. The triplet structure was determined to be 38.3 kcal/mol higher in energy than ground state **1a**. Notably, upon photoexcitation, the oxidation state of the iodine center in the long-lived triplet structure **1a*_T** remains unchanged as negligible spin density resides on the iodine center within triplet structure **1a*_T**. This is because

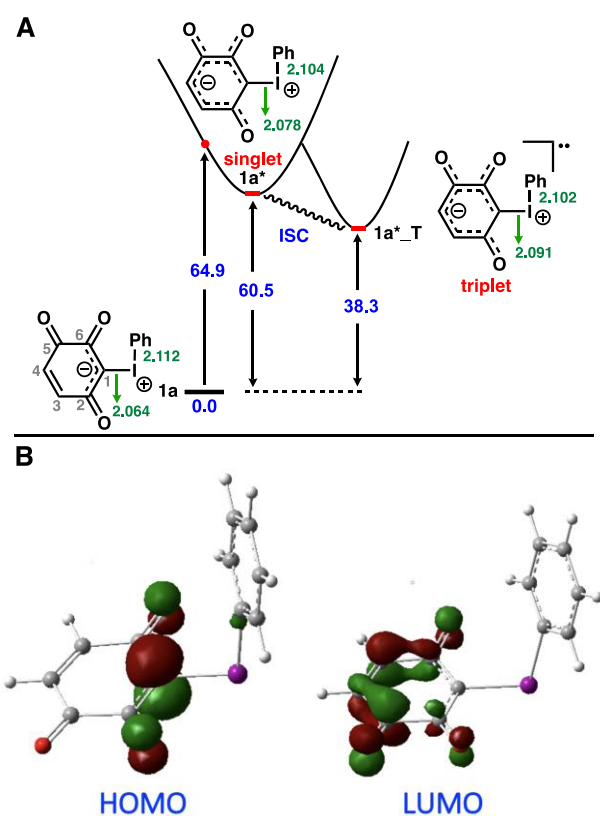


Figure 4. (A) Simplified Jablonski diagram showing the photochemical activation pathway leading to triplet structure **1a*_T** calculated by SMD/CAM-B3LYP/LANL2DZ,6-31G(d) in acetonitrile. Potential energies (blue) are given in kcal/mol and referenced to compound **1a**; selected bond distances (green) are given in Å. (B) Spatial plots of the HOMO and the LUMO for compound **1a**.

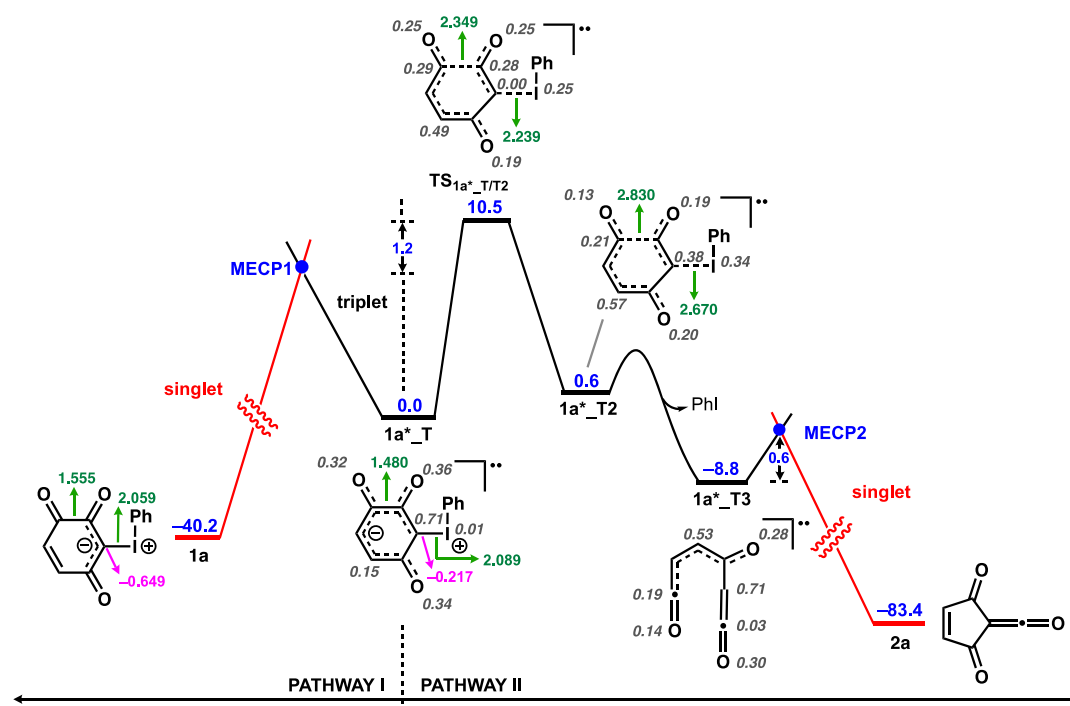


Figure 5. Free energy profiles studying competition between pathway I ($1a^*_T \rightarrow 1a$) and pathway II ($1a^*_T \rightarrow 2a + PhI$) calculated by SMD/M06-2X-D3/def2-TZVP/SMD/M06-2X-D3/LANL2DZ,6-31G(d) in acetonitrile. Spin densities derived from Mulliken population analysis of all triplet structures (gray); NPA partial charge (pink); and selected bond distances (green; Å) for some optimized structures are included. Free energies are given in kcal/mol and referenced to structure $1a^*_T$.

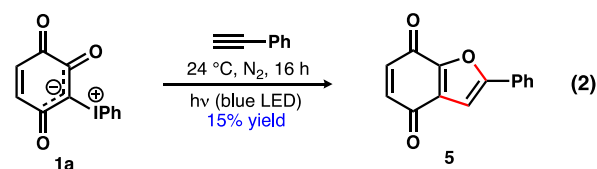
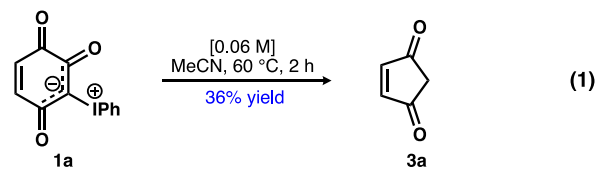
the presence of the C=C bond, which is stabilized by the conjugation with the carbonyl π system, leads to the preferential population of the $C^3=C^4$ π^* orbital in favor of the low-lying C–I σ^* orbital. It is important to compare this finding with the germane study investigating the photoexcitation of related, but less conjugated, ylide **1d** (Figure 1B).⁷ In the latter case, photoexcitation leads to the formal reduction of iodine(III) to iodine(II) within ensuing excited triplet structure $1d^*_T$ due to the occupation of a C–I σ^* orbital by the excited electron.

Triplet intermediate $1a^*_T$ may represent a branching point for at least two pathways (Figure 5). For example, this structure can undergo a redox process ($\Delta G^\ddagger = 10.5$ kcal/mol) via $TS_{1a^*_T/T2}$ to give species $1a^*_T2$, from which triplet organic intermediate $1a^*_T3$ may be formed following the loss of iodobenzene. The resultant intermediate is prone to cyclization to afford ketene **2a** on the singlet surface by crossing MECP2. We determined that this crossing point lies only 0.6 kcal/mol above structure $1a^*_T3$. Alternatively, triplet intermediate $1a^*_T$ may undergo a quenching process by passing through MECP1 to return starting material **1a**. MECP1 is computed to be 1.2 kcal/mol lower in energy than $TS_{1a^*_T/T2}$, which suggests that both the quenching and redox pathways are competitive.

Our calculations indicate that the productive photochemical pathway involving triplet structure $1a^*_T$ requires a much smaller activation energy barrier ($\Delta G^\ddagger = 10.5$ kcal/mol; Figure 5) relative to the thermal reaction via ground-state molecule **1a** ($\Delta G^\ddagger = 27.0$ kcal/mol; Table 2). These data are consistent with our aforementioned experimental findings which demonstrate that irradiation with visible light facilitates the formation of dione **3a**. The higher reactivity of the triplet structure can be attributed to the weaker I–C¹ bond within structure $1a^*_T$

compared to the equivalent bond within iodonium **1a**.²⁰ This is supported by the longer I–C¹ distance for intermediate $1a^*_T$ relative to ground-state singlet structure **1a** (2.089 vs 2.059 Å; Figure 5). Natural population analysis (NPA) reveals that the electron density on the C¹ atom decreases from –0.649 (**1a**) to –0.217 ($1a^*_T$). The greater electron density on the C¹ atom in **1a** results in it coordinating more strongly to the iodine(III) atom, making the iodine center in this structure less reactive toward reduction. This is supported by our calculations indicating that transition structure $TS_{1a^*_T/T2}$ occurs earlier than transition structure $TS_{1a/2a}$, which is consistent with the shorter I–C¹ distance within $TS_{1a^*_T/T2}$ relative to the equivalent bond within $TS_{1a/2a}$ (2.239 vs 2.804 Å; Figure 5 and Table 2).

In practice, we found that cyclopentenedione **3a** was most efficiently prepared by heating iodonium **1a** in acetonitrile at 60 °C (eq 1), which aligns with previous findings.^{2b}



Bimolecular photochemical reactions with molecule **1a** were not particularly efficient. For example, reactions of phenyliodonium **1a** and styrene performed in the presence of visible light gave a complex mixture of products. Furthermore, when we reacted substrate **1a** with phenylacetylene only low yields of heterocycle **5** were obtained (eq 2). This is comparable to the results of germane photochemical reactions employing UV light to convert substrates **1** into furanoquinones and furanonaphthoquinones.^{1,2b,4a} In an effort to understand the origins of the poor efficiency of this reaction of **1a**, we employed DFT calculations (Figure 6). The presence of a

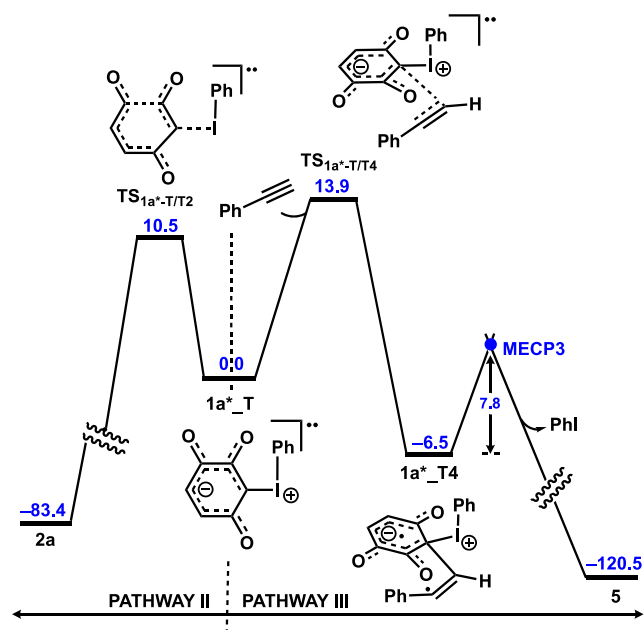


Figure 6. Free energy profiles studying competition between pathway III ($1a^*_T \rightarrow 5$) and pathway II ($1a^*_T \rightarrow 2a$) calculated by SMD/M06-2X-D3/def2-TZVP/SMD/M06-2X-D3/LANL2DZ,6-31G(d) in acetonitrile. Free energies are given in kcal/mol and referenced to structure $1a^*_T$.

single electron on the C^1 atom within biradical structure $1a^*_T$ makes this species prone to react with the alkyne via transition structure $TS_{1a^*_T/T4}$ which lies only 13.9 kcal/mol above $1a^*_T$. Resultant triplet structure $1a^*_T4$ can then cyclize on the singlet surface by overcoming the activation energy barrier associated with the triplet to singlet spin flip via MECP3 to form furanoquinone **5** exergonically. However, while the ring closure is predicted to be kinetically favorable, the barrier for the competing process that provides ketene **2a** is 3.4 kcal/mol lower in energy. The low yield obtained for heterocycle **5** may derive from this competition.²¹ It should be noted this competing pathway is not operative in the photochemical reaction of iodonium **1d** with styrene which proceeds in excellent yield (Figure 1B).⁷

Photoinduced Reactions Mediated by Ylide 1a. When THF solutions containing azodicarboxylate esters **6** were irradiated with visible light in the presence of iodonium **1a**, products **7** were synthesized in good to excellent yields (Figure 7A).^{22,23} Similar types of reactions of azodicarboxylate esters have been reported using UV irradiation, transition-metal-based photocatalysis, and *N*-hydroxyamide catalysts.²⁴ Our findings are consistent with molecule **1a** serving as a free radical initiator in its photoexcited state. Specifically, we

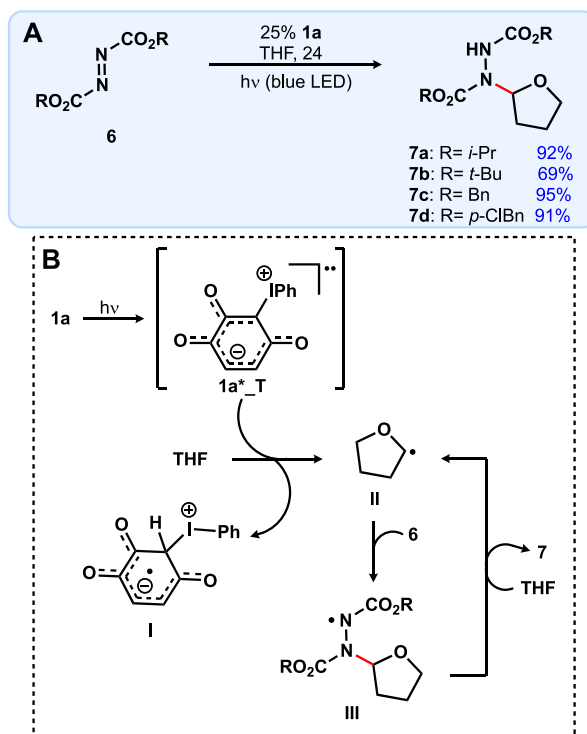


Figure 7. Photoinduced, phenyliodonium-promoted C–H functionalization of THF via HAT.

suggest that species $1a^*_T$ is capable of abstracting a hydrogen atom from THF and ensuing carbon-centered radical **II** adds to azodicarboxylate ester **6** to afford nitrogen-centered radical **III**. The latter is capable of abstracting a hydrogen atom from THF leading to a radical chain process (Figure 7B).²⁵

The results shown in Figure 7 suggest that triplet species $1a^*_T$ is sufficiently long-lived and reactive for it to serve as a radical generator in this transformation. To further support this hypothesis, we used DFT calculations to investigate the reaction of $1a^*_T$ with THF (Figure 8). Triplet $1a^*_T$ contains different reactive sites that have the capacity to generate organic radicals. We determined that the C^1 atom within intermediate $1a^*_T$, which has the highest spin density, is the most reactive site, and can produce a radical with the lowest activation energy barrier. Specifically, species $1a^*_T$ can abstract a hydrogen radical from THF with activation barriers comparable to those leading to ketene **2a** (within 0.2 kcal/mol). Thus, although $1a^*_T$ is highly reactive toward the latter pathway, the hydrogen atom transfer (HAT) reaction with THF is competitive and viable.

We found that iodonium **1a** also facilitates the photoinduced, Povarov-type reaction between *N,N*-dimethylaniline and *N*-phenylmaleimide (**8**) to afford tetrahydroquinoline **9**, albeit in moderate yield (eq 3). Our DFT calculations exploring the activation of *N,N*-dimethylaniline are consistent with species $1a^*_T$ promoting this transformation.²⁶ In addition, we also determined that molecule **1a** was capable of promoting an atom-transfer radical addition reaction between 1-octene (**10**) and bromotrichloromethane (eq 4). These results further support the involvement of SET processes when molecule **1a** undergoes photoactivation.

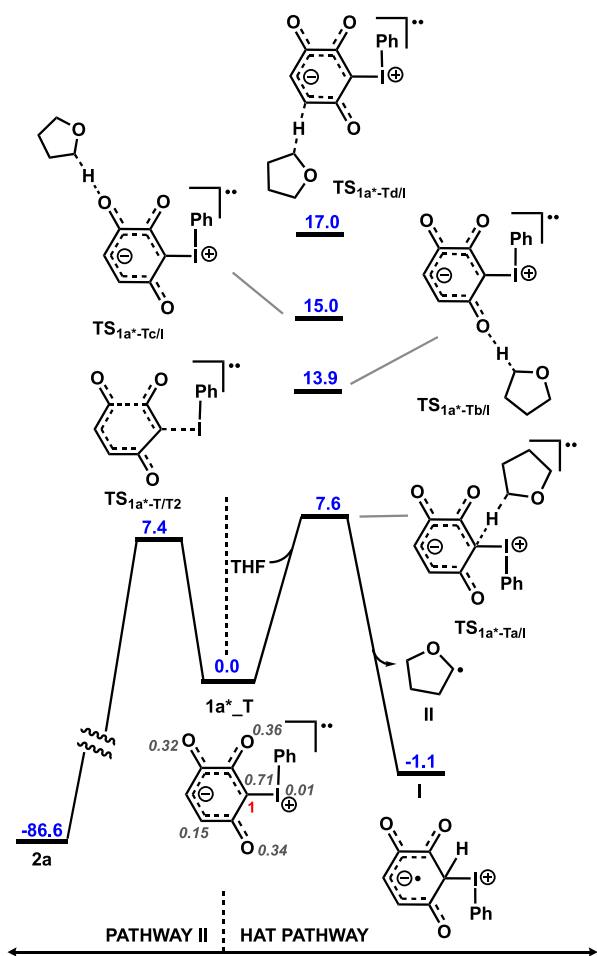
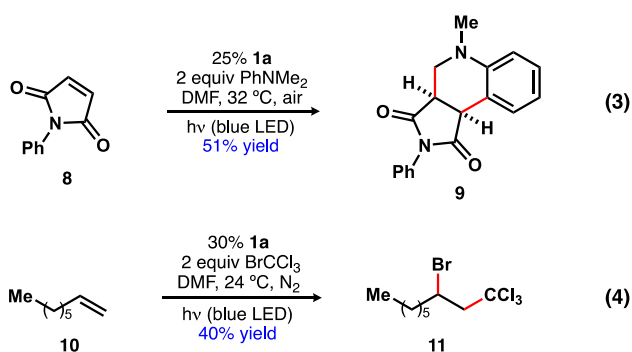


Figure 8. Free energy profiles studying the competition between conversions (a) $1a^*_T + \text{THF} \rightarrow \text{II} + \text{I}$ and $1a^*_T \rightarrow 2a$ in THF calculated by SMD/M06-2X-D3/def2-TZVP//SMD/M06-2X-D3/LANL2DZ,6-31G(d). Free energies are given in kcal/mol and referenced to structure $1a^*_T$.



CONCLUSIONS

We have extensively investigated the photochemical activation and reaction of a hydroxyquinone-derived phenyliodonium ylide in the presence of visible light. Our studies have revealed that iodonium $1a$ can undergo an original photochemical rearrangement. Furthermore, we have determined that, in its photoexcited state, triplet $1a^*_T$ is sufficiently long-lived and reactive to promote various SET processes, including HAT, a Povarov-type reaction, and atom-transfer radical addition chemistry. We anticipate that by developing a more complete

understanding of hydroxyquinone-derived phenyliodonium ylides, their photoactivation, and associated fundamental reactivity may serve to broaden the scope and applications of this interesting and relatively underutilized class of compounds in synthesis.

EXPERIMENTAL SECTION

General Information. NMR spectroscopic experiments were performed either on a Bruker Avance III NMR spectrometer operating at 400 MHz (^1H) and 100 MHz (^{13}C) or on a Bruker Avance III NMR spectrometer operating at 600 MHz (^1H) and 150 MHz (^{13}C). The deuterated solvents used were CDCl_3 , CD_3CN , and $\text{DMSO-}d_6$. Chemical shifts were recorded in ppm. Spectra were calibrated by assignment of the residual solvent peak to δ_{H} 7.26 and δ_{C} 77.16 for CDCl_3 , δ_{H} 1.94 and δ_{C} 1.32 for CD_3CN , and δ_{H} 2.50 and δ_{C} 39.52 for $\text{DMSO-}d_6$. Coupling constants (J) were recorded in Hz. Infrared spectroscopy was performed on a Shimadzu FTIR 8400s spectrometer, with samples analyzed as thin films on NaCl plates. High resolution mass spectra (HRMS) were recorded on either a Shimadzu LCMS-9030 Q-TOF mass spectrometer using an electrospray ionization (ESI) source in either the positive or negative modes or a Thermo Scientific Q-Exactive HF Orbitrap mass spectrometer equipped with HESI interface. Photochemical experiments were performed in either custom blue LED ($\lambda_{\text{max}} = 467 \text{ nm}$) photoreactor #1²⁷ (maintained at 24 °C) or custom blue LED ($\lambda_{\text{max}} = 467 \text{ nm}$) photoreactor #2 (maintained at 32 °C).²⁸ Blue LED strips were purchased from aliexpress.com. In each experiment, reaction vessels were placed within 3–4 cm from the light source; light filters were not used. All irradiation vessels were composed of borosilicate glass.

TLC was performed using Merck silica gel 60-F₂₅₄ plates. Developed TLC plates were visualized by UV absorbance (254 nm) or through application of heat to a plate stained with cerium molybdate $\{\text{Ce}(\text{NH}_4)_2(\text{NO}_3)_6, (\text{NH}_4)_6\text{Mo}_7\text{O}_{24}\cdot 4\text{H}_2\text{O}, \text{H}_2\text{SO}_4, \text{H}_2\text{O}\}$. Flash column chromatography was performed with flash grade silica gel (60 μm) and the indicated eluent in accordance with standard techniques.²⁹ THF, Et_2O , CH_2Cl_2 , PhMe, DMF, and CD_3CN were deaerated via a nitrogen sparge then dried using an Innovative Technology solvent purification system. Unless otherwise specified all reagents employed in these studies were used as received from Sigma-Aldrich, AK Scientific, Combi-Blocks, and Oakwood. Previously reported compounds $1b^{4a}$ and $1c^{2b}$ were prepared in accordance with literature procedures.

Computational Details. Gaussian 16³⁰ was used to fully optimize all the structures reported in this paper at the M06-2X level³¹ of density functional theory (DFT). Grimme empirical dispersion was added with the GD3 term on all the optimization calculations.³² For all the calculations, solvent effects were considered using the SMD solvation model for different solvents, including: CH_3CN , CHCl_3 , THF, and DMF.³³ The effective core potential of Hay and Wadt with a double- ξ valence basis set (LANL2DZ)³⁴ was chosen to describe iodine. Polarization functions were also added for I ($\xi_{\text{d}} = 0.289$).³⁵ The 6-31G(d) basis set was used for other atoms.³⁶ This basis set combination will be referred to as BS1. Frequency calculations were carried out at the same level of theory as those for the structural optimization. Transition structures were located using the Berny algorithm. Intrinsic reaction coordinate (IRC) calculations³⁷ were used to confirm the connectivity between transition structures and minima. To further refine the energies obtained from the SMD/M06-2X-D3/BS1 calculations, we carried out single-point energy calculations using the M06-2X-D3 functional method³⁸ for all the structures with a larger basis set (BS2). BS2 utilizes def2-TZVP³⁹ basis set on all atoms. Tight convergence criterion was also employed to increase the accuracy of the single point calculations. All thermodynamic data were calculated at the standard state (298.15 K and 1 atm).

In this work, the free energy for each species optimized by SMD/M06-2X-D3/BS1 in solution was calculated using the formula: $G = E(\text{BS2}) + G(\text{BS1}) - E(\text{BS1}) + \Delta G^{\text{latm} \rightarrow 1\text{M}}$; where $\Delta G^{\text{latm} \rightarrow 1\text{M}} = 1.89 \text{ kcal/mol}$ is the free-energy change for compression of 1 mol of an

ideal gas from 1 atm to the 1 M solution phase standard state. An additional correction to Gibbs free energies was made to consider solvent (THF) concentration where a THF is directly involved in transformations. In such a case, the free energy of a THF molecule is described as $G(\text{THF}) = E(\text{BS2}) + G(\text{BS1}) - E(\text{BS1}) + \Delta G^{\text{1atm} \rightarrow 1\text{M}} + RT \ln(12.2)$; where the last term corresponds to the free energy required to change the standard state of THF from 12.2 to 1 M.⁴⁰ The numerical correction value for THF was calculated to be 1.4 kcal/mol. TD-DFT calculations were performed using the SMD/CAM-B3LYP/BS1 level of theory in CH₃CN, which is specifically designed for investigating the nature of the excited states.⁴¹ Natural population analysis (NPA) was carried out using NBO6 software integrated into Gaussian 16.⁴² The respective minimum energy crossing points (MECPs) between singlet structure **1a** and triplet structure **1a*_T**; singlet structure **2a** and triplet structure **1a*_{T3}**; and singlet structure **5** and triplet structure **1a*_{T4}** were located using the code reported by Harvey and co-workers.⁴³

CrystalExplorer 17.5 was used to examine the arrangement molecules of complex **1a**.⁴⁴

X-ray Crystallography. Data for compound **1a** were collected at 100 K using Cu K α radiation (microsource, mirror monochromated) using an Agilent SuperNova diffractometer with Atlas detector. The structures were solved by direct methods with SHELXT-2014, refined using full-matrix least-squares routines against F^2 with SHELXL-2014,⁴⁵ and visualized using OLEX2.⁴⁶ All non-hydrogen atoms were refined anisotropically. All hydrogen atoms attached to carbon were placed in calculated positions and refined using a riding model with fixed C–H distances of 0.95 Å ($sp^2\text{CH}$). The thermal parameters of hydrogen atoms were estimated as $U_{\text{iso}}(\text{H}) = 1.2U_{\text{eq}}(\text{C})$. CCDC-2041504 contains the supplementary crystallographic data for compound **1a**. The data can be obtained free of charge from The Cambridge Crystallographic Data Centre via http://www.ccdc.cam.ac.uk/data_request/cif. Crystal data for compound **1a**: C₁₂H₇O₃, $M = 326.08$, triclinic, $a = 8.0768(3)$, $b = 11.5213(4)$, $c = 12.1793(4)$ Å, $\alpha = 71.418(3)$, $\beta = 87.592(3)$, $\gamma = 88.719(3)$ °, $U = 1073.27(7)$ Å³, $T = 100$ K, space group $P\bar{1}$ (no. 2), $Z = 4$, 18359 reflections measured, 4207 unique ($R_{\text{int}} = 0.0788$), $3694 > 4\sigma(F)$, $R = 0.0391$ (observed), $R_w = 0.1016$ (all data).

Synthesis of Products. Compound 1a. A mixture of PIDA (32.0 g, 99.9 mmol) in CH₂Cl₂ (120 mL) was added to a magnetically stirred solution of benzene-1,2,4-triol (6.00 g, 47.6 mmol) in CH₂Cl₂ (300 mL) maintained at 0 °C in air. After 0.25 h, the reaction mixture was warmed to room temperature. After 2 h, the reaction mixture was filtered and the red precipitate was collected. The filtrate was concentrated to ca. one-third of its volume and hexanes were added (100 mL) and the ensuing mixture was magnetically stirred. The red precipitate was collected and the combined solids were dried under a vacuum. This afforded the previously reported compound **1a** (11.2 g, 72% yield) as a red powder.² X-ray quality crystals were grown from CH₃CN/Et₂O. ¹H NMR (600 MHz, DMSO-*d*₆) δ 7.81 (d, $J = 7.7$ Hz, 2H), 7.52 (t, $J = 7.3$ Hz, 1H), 7.40 (t, $J = 7.7$ Hz, 2H), 6.94 (d, $J = 10.0$ Hz, 1H), 6.62 (d, $J = 10.0$ Hz, 1H) ppm. ¹³C{¹H} NMR (150 MHz, DMSO-*d*₆) δ 182.2, 177.3, 168.9, 139.9, 133.2, 132.6, 131.1, 130.6, 114.1, 97.8 ppm.

2-Cyclopentene-1,4-dione (3a). CH₃CN (200 mL) was added to a 250 mL round-bottomed flask containing compound **1a** (2.00 g, 6.13 mmol) and a stir bar in air. The flask was fitted with a condenser and the mixture was then heated at 60 °C. After 2 h, the reaction mixture was concentrated under reduced pressure and the ensuing residue was subjected to flash column chromatography (silica gel, 0–20% Et₂O/hexanes elution) to provide the previously reported compound (210 mg, 36% yield) as a colorless amorphous solid.² ¹H NMR (600 MHz, CDCl₃) δ 7.30 (s, 2H), 2.90 (s, 2H) ppm. ¹³C{¹H} NMR (150 MHz, CDCl₃) δ 199.7, 149.5, 40.5 ppm.

2-Phenylbenzofuran-4,7-dione (5). In a nitrogen-filled glovebox, phenylacetylene (2 mL) was added to a 4 mL screw-top vial containing compound **1a** (100 mg, 307 μ mol) and a stir bar. The vial was then capped and removed from the glovebox, placed in blue LED photoreactor #1 (switched off) and magnetically stirred. The vial was then irradiated and, after 14 h, the flask was removed from the

photoreactor. The reaction mixture was then subjected to flash column chromatography (silica gel, 0–5% EtOAc/hexanes elution) to provide previously reported compound **5** as a red solid (10 mg, 15% yield).⁴⁷ ¹H NMR (600 MHz, CDCl₃) δ 7.86 (d, $J = 7.3$ Hz, 2H), 7.54–7.44 (complex m, 3H), 7.07 (s, 1H), 6.77 (d, $J = 10.3$ Hz, 1H), 6.73 (d, $J = 10.4$ Hz, 1H) ppm. ¹³C{¹H} NMR (150 MHz, CDCl₃) δ 183.0, 174.4, 159.8, 149.7, 136.4, 130.31, 130.29, 129.1, 128.2, 125.5, 102.3 ppm.

General Procedure A: Synthesis of Compounds 7. In air, THF (5 mL) was added to a 20 mL screw-top vial containing compound **1a** (30 mg, 92 μ mol), the azodicarboxylate ester **6** (613 μ mol), and a stir bar. The vial was then capped and placed in blue LED photoreactor #1 (switched off) and magnetically stirred at 24 °C (Figure S1). The vial was then irradiated. After 5 h, compound **1a** (10 mg, 31 μ mol) was added and, after a further 5 h, compound **1a** (10 mg, 31 μ mol) was added. After a further 14 h, the vial was removed from the photoreactor. The reaction mixture was concentrated under reduced pressure and the ensuing residue was subjected to flash column chromatography.

Diisopropyl 1-(tetrahydrofuran-2-yl)hydrazine-1,2-dicarboxylate (7a). This reaction employed diisopropyl azodicarboxylate (DIAD) and followed General Procedure A. The ensuing residue obtained from the reaction mixture was subjected to flash column chromatography (silica gel, 0–20% EtOAc/hexanes elution) to provide previously reported compound **7a** as a colorless amorphous solid (155 mg, 92% yield).⁴⁸ ¹H NMR (600 MHz, CDCl₃) δ 6.60–6.28 (m, 1H), 5.96 (br s, 1H), 4.91 (sept, $J = 6$ Hz, 2H), 3.95 (q, $J = 6.9$ Hz, 1H), 3.71 (q, $J = 6.9$ Hz, 1H), 2.11–1.77 (complex m, 4H), 1.21 (br s, 12H) ppm. ¹³C{¹H} NMR (150 MHz, CDCl₃) δ 156.4, 155.0, 87.0, 70.5, 69.8, 68.6, 28.2, 25.3, 22.0, 21.9 ppm.

Di-tert-butyl 1-(tetrahydrofuran-2-yl)hydrazine-1,2-dicarboxylate (7b). This reaction employed di-tert-butyl azodicarboxylate and followed General Procedure A. The ensuing residue obtained from the reaction mixture was subjected to flash column chromatography (silica gel, 0–20% EtOAc/hexanes elution) to provide previously reported compound **7b** as a colorless amorphous solid (127 mg, 69% yield).⁴⁹ ¹H NMR (600 MHz, CDCl₃) δ 6.18 (br s, 1H), 5.95 (m, 1H), 3.99 (m, 1H), 3.77 (m, 1H), 2.07–2.00 (m, 3H), 1.83 (m, 1H), 1.49 (br s, 18H) ppm. ¹³C{¹H} NMR (150 MHz, CDCl₃) δ 155.6, 154.3, 87.2, 81.8, 81.1, 68.5, 28.2, 25.3 ppm; 8 signals observed.

Dibenzyl 1-(tetrahydrofuran-2-yl)hydrazine-1,2-dicarboxylate (7c). This reaction employed dibenzyl azodicarboxylate and followed General Procedure A. The ensuing residue obtained from the reaction mixture was subjected to flash column chromatography (silica gel, 0–30% EtOAc/hexanes elution) to provide previously unreported compound **7c** as a colorless amorphous solid (215 mg, 95% yield). ¹H NMR (600 MHz, CDCl₃) δ 7.32 (br s, 10H), 6.55 (br s, 1H), 6.02 (br s, 1H), 5.17 (br s, 4H), 3.95 (d, $J = 6.6$ Hz, 1H), 3.74 (q, $J = 7.1$ Hz, 1H), 2.19–1.77 (complex m, 4H) ppm. ¹³C{¹H} NMR (150 MHz, CDCl₃) δ 156.7, 155.6, 135.8, 128.8, 128.7, 128.6, 128.5, 128.4, 128.2, 88.0, 69.0, 68.6, 68.1, 28.6, 25.5 ppm; 15 signals observed. IR (NaCl) 3286, 2956, 2359, 1722, 1493, 1223, 1092, 1044, 1016, 805 cm⁻¹. HRMS (ESI) m/z [M + Na]⁺ Calcd for C₂₀H₂₂N₂O₅Na 393.1421, Found 393.1404.

Bis(4-chlorobenzyl) 1-(tetrahydrofuran-2-yl)hydrazine-1,2-dicarboxylate (7d). This reaction employed di-(4-chlorobenzyl)-azodicarboxylate (DCAD) and followed General Procedure A. The ensuing residue obtained from the reaction mixture was subjected to flash column chromatography (silica gel, 0–30% EtOAc/hexanes elution) to provide previously unreported compound **7d** as a colorless amorphous solid (245 mg, 91% yield). ¹H NMR (600 MHz, CDCl₃) δ 7.24 (br s, 8H), 6.44 (br s, 1H), 5.92 (br s, 1H), 5.07 (br s, 4H), 3.89 (m, 1H), 3.68 (q, $J = 7.2$ Hz, 1H), 2.03–1.79 (complex m, 4H) ppm. ¹³C{¹H} NMR (150 MHz, CDCl₃) δ 156.2, 155.2, 134.4, 134.3, 134.1, 134.0, 129.5, 129.4, 128.8, 128.7, 87.8, 68.8, 67.6, 67.0, 28.3, 25.2 ppm. IR (NaCl) 3286, 2957, 1723, 1493, 1242, 1225, 1093, 1046, 1016, 806 cm⁻¹. HRMS (ESI) m/z [M + Na]⁺ Calcd for C₂₀H₂₀Cl₂N₂O₅Na 461.0642, Found 461.0615.

5-Methyl-2-phenyl-3a,4,5,9b-tetrahydro-1H-pyrrolo[3,4-c]-quinoline-1,3(2H)-dione (9). In air, compound **1a** (28 mg, 86 μ mol)

was added to a 20 mL screw-top vial containing, *N*-phenylmaleimide (100 mg, 577 μmol), PhNMe_2 (140 mg, 1.15 mmol), DMF (2.5 mL), and a stir bar. The vial was then capped and placed in a water bath (suspended with Cu wire) maintained at 32 $^\circ\text{C}$ that was contained within blue LED photoreactor #2 (switched off) and magnetically stirred. The vial was then irradiated. After 5 h, compound **1a** (9.5 mg, 29 μmol) was added and, after a further 5 h, compound **1a** (9.5 mg, 29 μmol) was added. After a further 14 h, the vial was removed from the photoreactor. The reaction mixture was concentrated under reduced pressure and the ensuing residue was subjected to flash column chromatography (silica gel, 0–20% EtOAc/hexanes elution; 0.5% NEt_3 was present in the eluent) to provide a yellow solid. Recrystallization from Et_2O afforded previously reported compound **9** as a colorless solid (86 mg, 51% yield).⁵⁰ ^1H NMR (600 MHz, CDCl_3) δ 7.54 (d, J = 7.9 Hz, 1H), 7.44 (t, J = 7.9 Hz, 2H), 7.36 (t, J = 7.4 Hz, 1H), 7.31–7.22 (complex m, 3H), 6.92 (t, J = 7.9 Hz, 1H), 6.76 (d, J = 7.9 Hz, 1H), 4.17 (d, J = 9.7 Hz, 1H), 3.62 (dd, J = 11.5, 2.6 Hz, 1H), 3.54 (dt, J = 9.3, 3.0 Hz, 1H), 3.13 (dd, J = 11.5, 4.4 Hz, 1H), 2.85 (s, 3H) ppm. $^{13}\text{C}\{^1\text{H}\}$ NMR (150 MHz, CDCl_3) δ 177.7, 175.8, 148.5, 132.0, 130.4, 129.0, 128.7, 128.5, 126.3, 119.7, 118.6, 112.6, 50.7, 43.6, 42.2, 39.5 ppm.

3-Bromo-1,1,1-trichlorononane (11). In a nitrogen-filled glovebox, compound **1a** (32.5 mg, 100 μmol) was added to a Schlenk flask containing, 1-octene (112 mg, 1.00 mmol), BrCCl_3 (397 mg, 2.00 mmol), CH_2Cl_2 (5 mL), and a stir bar. The flask was then stoppered and removed from the glovebox, placed in blue LED photoreactor #1 (switched off) and magnetically stirred. The flask was then irradiated. After 3 h, compound **1a** (32.5 mg, 100 μmol) was added under a stream of Ar and, after a further 3 h, compound **1a** (32.5 mg, 100 μmol) was added under a stream of Ar. After a further 15 h, the flask was removed from the photoreactor. The reaction mixture was exposed to air and concentrated under reduced pressure and the ensuing residue was subjected to flash column chromatography (silica gel, hexanes elution) to provide previously reported compound **11** as a colorless oil (125 mg, 40% yield).⁵¹ ^1H NMR (400 MHz, CDCl_3) δ 4.32 (m, 1H), 3.33 (ABq, J = 15.9 Hz, 2H), 1.98 (m, 2H), 1.54 (m, 2H), 1.32 (m, 6H), 0.89 (t, J = 6.7 Hz, 3H) ppm. $^{13}\text{C}\{^1\text{H}\}$ NMR (100 MHz, CDCl_3) δ 97.4, 62.9, 49.1, 36.7, 31.7, 28.6, 27.3, 22.7, 14.2 ppm.

■ ASSOCIATED CONTENT

SI Supporting Information

The Supporting Information is available free of charge at <https://pubs.acs.org/doi/10.1021/acs.joc.0c02592>.

Additional experimental information and compound characterization data (PDF)

Accession Codes

CCDC 2041504 contains the supplementary crystallographic data for this paper. These data can be obtained free of charge via www.ccdc.cam.ac.uk/data_request/cif, or by emailing data_request@ccdc.cam.ac.uk, or by contacting The Cambridge Crystallographic Data Centre, 12 Union Road, Cambridge CB2 1EZ, UK; fax: +44 1223 336033.

■ AUTHOR INFORMATION

Corresponding Authors

Alireza Ariaifard – School of Natural Sciences – Chemistry, University of Tasmania, Hobart, Tasmania 7001, Australia; orcid.org/0000-0003-2383-6380; Email: alireza.ariaifard@utas.edu.au

Alex C. Bissember – School of Natural Sciences – Chemistry, University of Tasmania, Hobart, Tasmania 7001, Australia; orcid.org/0000-0001-5515-2878; Email: alex.bissember@utas.edu.au

Authors

Mona Jalali – School of Natural Sciences – Chemistry, University of Tasmania, Hobart, Tasmania 7001, Australia

Curtis C. Ho – School of Natural Sciences – Chemistry, University of Tasmania, Hobart, Tasmania 7001, Australia; orcid.org/0000-0002-7555-0635

Rebecca O. Fuller – School of Natural Sciences – Chemistry, University of Tasmania, Hobart, Tasmania 7001, Australia; orcid.org/0000-0003-3926-8680

Nigel T. Lucas – Department of Chemistry, University of Otago, Dunedin, Otago 9054, New Zealand; orcid.org/0000-0002-4944-9875

Complete contact information is available at: <https://pubs.acs.org/doi/10.1021/acs.joc.0c02592>

Notes

The authors declare no competing financial interest.

■ ACKNOWLEDGMENTS

We gratefully acknowledge the University of Tasmania School of Natural Sciences – Chemistry and an Australian Research Council (ARC) Discovery Project Grant (DP200101714) for funding, the University of Tasmania Central Science Laboratory for providing access to NMR spectroscopy services, and the generous allocation of computing time from the Australian National Computing Infrastructure and University of Tasmania. R.O.F.'s contributions were supported by an ARC Discovery Early Career Research Award (DE180100112). N.T.L. acknowledges financial support by the MacDiarmid Institute for Advanced Materials and Nanotechnology, and the Marsden Fund Council, managed by the Royal Society Te Apārangi, New Zealand.

■ REFERENCES

- (1) For a review on phenyliodonium zwitterions and their applications in synthesis, see: Varvoglis, A. In *Hypervalent Iodine in Synthesis*; Katritzky, A. R., Meth-Cohn, O., Rees, C. W., Eds.; Academic House: San Diego, 1997; pp 179–199.
- (2) For representative early examples, see: (a) Hatzigrigoriou, E.; Spyroudis, S.; Varvoglis, A. Derivatives of 1,4-Naphthoquinone via 3-(Phenyliodonio)-1,2,4-trioxo-1,2,3,4-tetrahydronaphthalene. *Liebigs Ann. Chem.* **1989**, 1989, 167–170. (b) Papoutsis, I.; Spyroudis, S.; Varvoglis, A. The chemistry of 2-oxido-3-phenyliodonio-1,4-benzoquinones: Transformation to 2-cyclopentene-1,4-diones and cycloadditions. *Tetrahedron Lett.* **1994**, 35, 8449–8452.
- (3) Alcock, N. W.; Bozopoulos, A. P.; Hatzigrigoriou, E.; Varvoglis, A. Structures of Two Phenyliodonium Ylides. *Acta Crystallogr., Sect. C: Cryst. Struct. Commun.* **1990**, 46, 1300–1303.
- (4) For selected examples, see: (a) Wu, C.; Johnson, R. K.; Mattern, M. R.; Wong, J. C.; Kingston, D. G. I. Synthesis of Furanonaphthoquinones with Hydroxyamino Side Chains. *J. Nat. Prod.* **1999**, 62, 963–968. (b) Glinis, E.; Malamidou-Xenikaki, E.; Skouros, H.; Spyroudis, S.; Tsanakopoulou, M. Arylation of lawsone through BF_3 -mediated coupling of its phenyliodonium ylide with activated arenes and aromatic aldehydes. *Tetrahedron* **2010**, 66, 5786–5792. (c) Malamidou-Xenikaki, E.; Spyroudis, S.; Tsovaltzi, E.; Bakalbassis, E. G. Cycloaddition Reactions of Indanedione ketene with Electron-Rich Dienophiles: An Experimental and a Theoretical Study. *J. Org. Chem.* **2016**, 81, 2383–2398. (d) Jiang, J.; Li, P.; Zhao, J.; Liu, B.; Li, X. Iodonium Ylides as Carbene Precursors in Rh(III)-Catalyzed C–H Activation. *Org. Lett.* **2020**, 22, 7475–7479.
- (5) For representative examples, see: (a) Koulouri, S.; Malamidou-Xenikaki, E.; Spyroudis, S.; Tsanakopoulou, M. Studies on the Reactivity of Phenyliodonium Ylide of 2-Hydroxy-1,4-Naphthoquinone: Reactions with Indole Derivatives and Other C-Nucleophiles. *J.*

Org. Chem. **2005**, *70*, 8780–8784. (b) Malamidou-Xenikaki, E.; Spyroudis, S.; Tsanakopoulou, M.; Krautscheid, H. Reactivity of Indanedione Ketene Dimer with Amines. *J. Org. Chem.* **2007**, *72*, 502–508.

(6) Bakalbassis, E. G.; Spyroudis, S.; Tsipis, C. A. Ketene Formation or Phenyl-Group Migration as the Favorable Intramolecular Rearrangement in Phenyliodonium Ylides of Hydroxyquinones. *Eur. J. Org. Chem.* **2008**, *2008*, 1783–1788.

(7) Chidley, T.; Jameel, I.; Rizwan, S.; Peixoto, P. A.; Pouységu, L.; Ouideau, S.; Hopkins, W. S.; Murphy, G. K. Blue LED Irradiation of Iodonium Ylides Gives Diradical Intermediates for Efficient Metal-free Cyclopropanation with Alkenes. *Angew. Chem., Int. Ed.* **2019**, *58*, 16959–16965.

(8) Gogonas, E. P.; Hadjjarapoglou, L. P. [3 + 2]-Cycloaddition reactions of 2-phenyliodonio-5,5-dimethyl-1,3-dioxacyclohexanemethylide. *Tetrahedron Lett.* **2000**, *41*, 9299–9303.

(9) Fuller, R. O.; Griffith, C. S.; Koutsantonis, G. A.; Lapere, K. M.; Skelton, B. W.; Spackman, M. A.; White, A. H.; Wild, D. A. Supramolecular interactions between hexabromoethane and cyclopentadienyl ruthenium bromides: Halogen bonding or electrostatic organisation? *CrystEngComm* **2012**, *14*, 804–811.

(10) Hirshfeld analysis was performed, and the data obtained support that the crystal packing derives from more than just the close I–O interactions. For further details, see Figures S1 and S2 (Supporting Information).

(11) Heinen, F.; Engelage, E.; Cramer, C. J.; Huber, S. M. Hypervalent Iodine(III) Compounds as Biaxial Halogen Bond Donors. *J. Am. Chem. Soc.* **2020**, *142*, 8633–8640.

(12) In an equivalent experiment employing phenyliodonium **1b**, we determined that this substrate did not react after 24 h under the same reaction conditions.

(13) Al, N.; Stolley, R. M.; Staudaher, N. D.; Vanderlinden, R. T.; Louie, J. Electronic Effect of Ligands on the Stability of Nickel–Ketene Complexes. *Organometallics* **2018**, *37*, 3750–3755.

(14) Notably, it was determined that an alternative stepwise pathway in which the elimination of iodobenzene generates a carbene intermediate that undergoes a Wolff-type rearrangement was kinetically disfavored ($1a \rightarrow 2a$: $\Delta G_{\text{calc}}^{\ddagger} = 40.6$ kcal/mol) (ref 6).

(15) Jiang, H.; Sun, T.-Y.; Wang, X.; Xie, Y.; Zhang, X.; Wu, Y.-D.; Schaefer, H. F. A Twist of the Twist Mechanism, 2-Iodoxybenzoic Acid (IBX)-Mediated Oxidation of Alcohol Revisited: Theory and Experiment. *Org. Lett.* **2017**, *19*, 6502–6505.

(16) Zhao, Y.; Truhlar, D. G. A new local density functional for main-group thermochemistry, transition metal bonding, thermochemical kinetics, and noncovalent interactions. *J. Chem. Phys.* **2006**, *125*, 194101.

(17) Figure 3 shows the most favorable reaction pathway that we identified computationally. Alternative possibilities for transformation of **2a** \rightarrow **3a** were also explored. For further details, see Figure S3 (Supporting Information).

(18) We determined that the absorption maximum for phenyliodonium **1b** is 414 nm employing UV–vis spectroscopy.

(19) Investigations of the third and fourth excited states of **1a** at two shorter wavelengths (346 and 299 nm) were ignored because each have negligible oscillator strengths. For further details, see pS4 (Supporting Information).

(20) This is further supported by energy decomposition analysis of $TS_{1a/2a}$ and $TS_{1a^*_{-T}/T2}$. For further details, see Figure S4 (Supporting Information).

(21) Indeed, in our laboratory experiments, dione **3a** was present in the crude reaction mixture, as judged by ^1H NMR spectroscopy.

(22) In control experiments, we determined <5% yield of product **7a** was obtained when the reaction was performed either in the absence of light or in the absence of phenyliodonium **1a**.

(23) When THF solutions containing diisopropyl azodicarboxylate (**6a**) were irradiated with visible light in the presence of either iodonium **1b** or iodonium **1c**, as per General Procedure A, product **7a** was synthesized in 89% and 48% yields, respectively.

(24) See, for example: (a) Schenck, G. O.; Formanek, H. Zur Strahlenchemie des Azodicarbonesters. *Angew. Chem.* **1958**, *70*, 505. (b) Cookson, R. C.; Stevens, J. D. R.; Watts, C. T. Photochemical Reaction of Diethyl Azodicarboxylate with Ethers and Alcohols. *Chem. Commun.* **1965**, 259–260. (c) Askani, R. Zur Reaktion von Cyclohexadien-(1,3) mit Azodicarbonsäure-diäthylester. *Chem. Ber.* **1965**, *98*, 2551–2555. (d) Ryu, I.; Tani, A.; Fukuyama, T.; Ravelli, D.; Montanaro, S.; Fagnoni, M. Efficient C–H/C–N and C–H/C–CO–N Conversion via Decatungstate-Photoinduced Alkylation of Diisopropyl Azodicarboxylate. *Org. Lett.* **2013**, *15*, 2554–2557.

(25) Grochowski, E.; Boleslawska, T.; Jurczak, J. Reaction of Diethyl Azodicarboxylate with Ethers in the Presence of *N*-Hydroxyimides as Catalysts. *Synthesis* **1977**, *10*, 718–720.

(26) For the results of our DFT study investigating this Povarov-type reaction, see Figure S5 (Supporting Information).

(27) Ranieri, A. M.; Burt, L. K.; Stagni, S.; Zacchini, S.; Skelton, B. W.; Ogden, M. I.; Bissember, A. C.; Massi, M. Anionic Cyclo-metalated Platinum(II) Tetrazolato Complexes as Viable Photoredox Catalysts. *Organometallics* **2019**, *38*, 1108–1117.

(28) Nicholls, T. P.; Robertson, J. C.; Gardiner, M. G.; Bissember, A. C. Identifying the potential of pulsed LED irradiation in synthesis: copper-photocatalysed C–F functionalisation. *Chem. Commun.* **2018**, *54*, 4589–4592.

(29) Still, W. C.; Kahn, M.; Mitra, A. Rapid chromatographic technique for preparative separations with moderate resolution. *J. Org. Chem.* **1978**, *43*, 2923–2925.

(30) Frisch, M. J.; Trucks, G. W.; Schlegel, H. B.; Scuseria, G. E.; Robb, M. A.; Cheeseman, J. R.; Scalmani, G.; Barone, V.; Petersson, G. A.; Nakatsuji, H.; Li, X.; Caricato, M.; Marenich, A. V.; Bloino, J.; Janesko, B. G.; Gomperts, R.; Mennucci, B.; Hratchian, H. P.; Ortiz, J. V.; Izmaylov, A. F.; Sonnenberg, J. L.; Williams-Young, D.; Ding, F.; Lipparini, F.; Egidi, F.; Goings, J.; Peng, B.; Petrone, A.; Henderson, T.; Ranasinghe, D.; Zakrzewski, V. G.; Gao, J.; Rega, N.; Zheng, G.; Liang, W.; Hada, M.; Ehara, M.; Toyota, K.; Fukuda, R.; Hasegawa, J.; Ishida, M.; Nakajima, T.; Honda, Y.; Kitao, O.; Nakai, H.; Vreven, T.; Throssell, K.; Montgomery, J. A.; Peralta, J. E.; Ogliaro, F.; Bearpark, M. J.; Heyd, J. J.; Brothers, E. N.; Kudin, K. N.; Staroverov, V. N.; Keith, T. A.; Kobayashi, R.; Normand, J.; Raghavachari, K.; Rendell, A. P.; Burant, J. C.; Iyengar, S. S.; Tomasi, J.; Cossi, M.; Millam, J. M.; Klene, M.; Adamo, C.; Cammi, R.; Ochterski, J. W.; Martin, R. L.; Morokuma, K.; Farkas, O.; Foresman, J. B.; Fox, D. J. *Gaussian 16*, Revision B.01; Gaussian, Inc.: Wallingford, CT, 2016.

(31) (a) Lee, C. T.; Yang, W. T.; Parr, R. G. Development of the Colic-Salvetti Correlation-energy Formula into a Functional of the Electron Density. *Phys. Rev. B: Condens. Matter Mater. Phys.* **1988**, *37*, 785–789. (b) Miehlich, B.; Savin, A.; Stoll, H.; Preuss, H. Results Obtained with the Correlation Energy Density Functionals of Becke and Lee, Yang and Parr. *Chem. Phys. Lett.* **1989**, *157*, 200–206. (c) Becke, A. D. J. Density Functional Thermochemistry.III. The Role of Exact Exchange. *J. Chem. Phys.* **1993**, *98*, 5648–5652.

(32) Grimme, S.; Antony, J.; Ehrlich, S.; Kreig, H. A Consistent and Accurate Ab initio Parametrization of Density Functional Dispersion Correction (DFT-D) for the 94 Elements H–Pu. *J. Chem. Phys.* **2010**, *132*, 154104.

(33) Marenich, A. V.; Cramer, C. J.; Truhlar, D. G. Universal Solvation Model Based on Solute Electron Density and on a continuum Model of the Solvent defined by the Bulk Dielectric Constant and Atomic Surface Tensions. *J. Phys. Chem. B* **2009**, *113*, 6378–6396.

(34) (a) Hay, P. J.; Wadt, W. R. Ab initio Effective Core Potentials for Molecular Calculations. Potentials for the Transition Metal Atoms Sc to Hg. *J. Chem. Phys.* **1985**, *82*, 270–283. (b) Wadt, W. R.; Hay, P. J. Ab initio Effective Core Potentials for Molecular Calculations. Potentials for Main Group elements Na to Bi. *J. Chem. Phys.* **1985**, *82*, 284–298.

(35) Ehlers, A. W.; Dapprich, M. S.; Gobbi, A.; Höllwarth, A.; Jonas, V.; Köhler, K. F.; Stegmann, R.; Veldkamp, A.; Frenking, G. A Set of f-polarization Functions for Pseudo-potential Basis Sets of the

Transition Metals Sc, Cu, Y, Ag, La, Au. *Chem. Phys. Lett.* **1993**, *208*, 111–114.

(36) Hariharan, P. C.; Pople, J. A. The Influence of Polarization Functions on Molecular Orbital Hydrogenation Energies. *Theor. Chim. Acta* **1973**, *28*, 213–222.

(37) (a) Fukui, K. J. Formulation of the Reaction coordinate. *J. Phys. Chem.* **1970**, *74*, 4161–4163. (b) Fukui, K. The Path of The Chemical Reactions -The IRC Approach. *Acc. Chem. Res.* **1981**, *14*, 363–368.

(38) Zhao, Y.; Truhlar, D. G. Density Functionals with Broad Applicability in Chemistry. *Acc. Chem. Res.* **2008**, *41*, 157–167.

(39) Weigend, F.; Furche, F.; Ahlrichs, R. J. Gaussian Basis Sets of Quadruple Zeta Valence Quality for Atoms H-Kr. *J. Chem. Phys.* **2003**, *119*, 12753–12762.

(40) (a) Bryantsev, V. S.; Diallo, M. S.; Goddard, W. A., III Calculation of solvation free energies of charged solutes using mixed cluster/continuum models. *J. Phys. Chem. B* **2008**, *112*, 9709–9719.

(b) Keith, J. A.; Carter, E. A. Quantum Chemical Benchmarking, Validation, and Prediction of Acidity Constants for Substituted Pyridinium Ions and Pyridinyl Radicals. *J. Chem. Theory Comput.* **2012**, *8*, 3187–3206.

(41) Yanai, T.; Tew, D. P.; Handy, N. C. A new Hybrid Exchange-correlation functional Using the Coulomb-attenuating Method (CAM-B3LYP). *Chem. Phys. Lett.* **2004**, *393*, 51–57.

(42) Glendening, E. D.; Badenhoop, J. K.; Reed, A. E.; Carpenter, J. E.; Bohmann, J. A.; Morales, C. M.; Landis, C. R.; Weinhold, F. *Natural Bond Order 6.0*; Theoretical Chemistry Institute, University of Wisconsin: Madison, WI, 2013. <http://nbo6.chem.wisc.edu>.

(43) Harvey, J. N.; Aschi, M.; Schwarz, H.; Koch, W. A hybrid approach for locating minimum energy crossing points between non-interacting potential energy surfaces. *Theor. Chem. Acc.* **1998**, *99*, 95–99.

(44) Wolff, S. K.; Grimwood, D. J.; McKinnon, J. J.; Turner, M. J.; Jayatilaka, D.; Spackman, M. A. *CrystalExplorer 17.5*; University of Western Australia, 2012.

(45) Sheldrick, G. M. *SHELXT* - Integrated space-group and crystal-structure determination. *Acta Crystallogr., Sect. A: Found. Adv.* **2015**, *A71*, 3–8.

(46) Dolomanov, O. V.; Bourhis, L. J.; Gildea, R. J.; Howard, J. A. K.; Puschmann, H. *OLEX2*: a complete structure solution, refinement and analysis program. *J. Appl. Crystallogr.* **2009**, *42*, 339–341.

(47) Zhang, L.; Cao, T.; Jiang, H.; Zhu, S. Deconstructive Reorganization: De Novo Synthesis of Hydroxylated Benzofuran. *Angew. Chem., Int. Ed.* **2020**, *59*, 4670–4677.

(48) Lee, D.; Otte, R. D. Transition-Metal-Catalyzed Aldehydic C–H Activation by Azodicarboxylates. *J. Org. Chem.* **2004**, *69*, 3569–3571.

(49) Feng, G.; Wang, X.; Jin, J. Decarboxylative C–C and C–N Bond Formation by Ligand-Accelerated Iron Photocatalysis. *Eur. J. Org. Chem.* **2019**, *2019*, 6728–6732.

(50) Nicholls, T. P.; Constable, G. E.; Robertson, J. C.; Gardiner, M. G.; Bissember, A. C. Brønsted Acid Cocatalysis in Copper(I)-Photocatalyzed α -Amino C–H Bond Functionalization. *ACS Catal.* **2016**, *6*, 451–457.

(51) Nicholls, T. P.; Burt, L. K.; Simpson, P. V.; Massi, M.; Bissember, A. C. Tricarbonyl rhenium(I) tetrazolato and N-heterocyclic carbene complexes: versatile visible-light-mediated photoredox catalysts. *Dalton Trans.* **2019**, *48*, 12749–12754.